Molecular Cell
Article

Structure of Human RNase H1 Complexed with an RNA/DNA Hybrid: Insight into HIV Reverse Transcription

Marcin Nowotny,[1] Sergei A. Gaidamakov,[2] Rodolfo Ghirlando,[1] Susana M. Cerritelli,[2] Robert J. Crouch,[2] and Wei Yang[1,*]
[1]Laboratory of Molecular Biology, National Institute of Diabetes and Digestive and Kidney Diseases
[2]Laboratory of Molecular Genetics, National Institute of Child Health and Human Development
National Institutes of Health, Bethesda, MD 20892, USA
*Correspondence: wei.yang@nih.gov
DOI 10.1016/j.molcel.2007.08.015

SUMMARY

We report here crystal structures of human RNase H1 complexed with an RNA/DNA substrate. Unlike *B. halodurans* RNase H1, human RNase H1 has a basic protrusion, which forms a DNA-binding channel and together with the conserved phosphate-binding pocket confers specificity for the B form and 2′-deoxy DNA. The RNA strand is recognized by four consecutive 2′-OH groups and cleaved by a two-metal ion mechanism. Although RNase H1 is overall positively charged, the substrate interface is neutral to acidic in character, which likely contributes to the catalytic specificity. Positions of the scissile phosphate and two catalytic metal ions are interdependent and highly coupled. Modeling of HIV reverse transcriptase (RT) with RNA/DNA in its RNase H active site suggests that the substrate cannot simultaneously occupy the polymerase active site and must undergo a conformational change to toggle between the two catalytic centers. The region that accommodates this conformational change offers a target to develop HIV-specific inhibitors.

INTRODUCTION

RNase H is an endonuclease that specifically hydrolyzes the RNA strand in RNA/DNA hybrids. It requires divalent metal ions, preferably Mg^{2+}, for catalysis. Two types of RNases H, H1 and H2, have been identified. They share a similar overall fold but differ in the active site configuration and substrate preference. RNase H1 (subsequently referred to as RNase H) is found in many forms of life from bacteria and viruses to humans. Cellular RNase H is thought to remove RNA primers from Okazaki fragments but is not the only enzyme with such an activity (Kogoma and Foster, 1998). It has also been shown to process R loops to modulate replication initiation and restore DNA topology (Broccoli et al., 2004). In unicellular organisms, deletion of RNase H slows growth rate with no lethal effect, but RNase H knockout mice die during embryogenesis due to the failure of mitochondrial DNA replication (Cerritelli et al., 2003). Retroviral reverse transcriptase (RT) contains an RNase H domain, whose activity is essential for reverse transcription to convert a single-stranded RNA (ssRNA) viral genome into double-stranded DNA (dsDNA) (Hughes et al., 1998). Any mutations that inactivate RNase H inhibit reverse transcription (Repaske et al., 1989; Tisdale et al., 1991). Therefore, RNase H is an attractive and actively explored anti-HIV drug target. A number of RNase H inhibitors have been identified (Klumpp and Mirzadegan, 2006), but as of now none has entered clinical trials.

Crystal structures of *E. coli* RNase H were first determined in 1990 and revealed a novel fold, which consists of a five-stranded β sheet flanked on both faces by α helices (Katayanagi et al., 1990; Yang et al., 1990). The active site is composed of four carboxylate residues—D10, E48, D70, and D134. This fold and two key active site aspartates (D10 and D70) were later identified to be common among the integrase superfamily, which includes retroviral integrases, transposases, RuvC, and Argonaute (Rice and Baker, 2001; Tolia and Joshua-Tor, 2007; Yang and Steitz, 1995).

The first crystal structures of an RNA/DNA substrate complex were solved using the catalytic domain of *Bacillus halodurans* RNase H (Bh-RNase HC) (Nowotny et al., 2005). They showed that the RNA strand of the hybrid is recognized by the protein through extensive contacts with 2′-OH groups. DNA strand is recognized by its ability to adopt a B form conformation. In the active site, two magnesium ions, termed A and B, were observed. Catalysis most probably occurs through the two-metal ion mechanism, which was first proposed by Steitz and Steitz in 1993 and has since been found in all polymerases, a large number of nucleases, and some catalytic RNAs (Steitz and Steitz, 1993; Yang et al., 2006). The ensuing crystal structures of Bh-RNase HC complexed with the reaction product and intermediate mimic revealed the

course of the hydrolytic reaction (Nowotny and Yang, 2006). It has been proposed that the A site Mg^{2+} activates the attacking nucleophile, the B site Mg^{2+} destabilizes the substrate, and A and B together stabilize the transition state and facilitate product release.

Like all eukaryotic RNases H, the human enzyme contains an N-terminal RNA and RNA/DNA hybrid-binding domain (RHBD) of ~50 aa (Cerritelli and Crouch, 1995), which enhances the processivity of RNase H (Gaidamakov et al., 2005). A flexible linker of ~60 residues connects the N-terminal RHBD and the C-terminal catalytic domain of ~150 aa. Based on the sequence homology, the residues D145, E186, D210, and D274 were predicted to form the active site. Mutagenesis studies confirmed that D145, E186, and D210 are essential for the enzymatic activity (Wu et al., 2001).

Human RNase H is predicted to contain a "basic protrusion," which is present in the *E. coli* enzyme but absent in Bh-RNase H and HIV RT (Cerritelli and Crouch, 1998). Deletion of 18 residues from the basic protrusion in *E. coli* RNase H reduced the affinity for RNA/DNA hybrids by 40-fold and inactivated the enzyme (Haruki et al., 1997). Interestingly, *E. coli* RNase H with a smaller deletion (13 residues) in the same region lost the Mg^{2+}-dependent activity but was capable of Mn^{2+}-dependent cleavage (Keck and Marqusee, 1996). The structures of the RNA/DNA hybrid observed in the Bh-RNase HC complex cannot be readily modeled into the structure of *E. coli* RNase H without major collisions with the basic protrusion. How *E. coli* and Hs-RNase H interact with RNA/DNA hybrids thus remains unknown. Moreover, since the basic protrusion is also absent in HIV RT, the difference in substrate recognition between human and viral RNases H may be instrumental in rational design of HIV RNase H inhibitors. The deleterious effects of RNase H knockout in mice indicate that the human enzyme probably is essential. Any drug that targets HIV RNase H has to be viral specific to avoid toxicity to humans.

After futile attempts to crystallize *E. coli* and mouse RNase H (full-length or linker-region deletion forms) complexed with RNA/DNA substrates, we succeeded in cocrystallization of the catalytic domain of human RNase H (Hs-RNase HC). Reported here are three crystal structures of Hs-RNase HC in complex with RNA/DNA hybrids. These structures reveal the role of basic protrusion in substrate recognition, the key differences between human and HIV RNase H, and suggest rational approaches to design HIV-specific inhibitors.

RESULTS AND DISCUSSION

Structure Determination of Hs-RNase HC-Substrate Complexes

Hs-RNase HC (residues 136–286) was expressed in *E. coli* and purified by affinity- and ion-exchange chromatography. Amino acid substitutions in the active site, D210N or D274N, were engineered to prevent degradation of the RNA/DNA substrate during crystallization. Only the D210N mutant protein lost both Mg^{2+}- and Mn^{2+}-dependent activity (see Figure S1 in the Supplemental Data available with this article online) and thus was chosen for crystallization trials. The protein exhibited some solubility problems. For crystallization, protein samples were concentrated either in 1 M NaCl or after addition of RNA/DNA hybrids to the diluted protein solutions.

Crystallization of apo protein and protein complexed with substrate was attempted. Crystals were obtained only from the D210N protein complexed with 14-mer, 18-mer, and 20-mer RNA/DNA hybrids. They belonged to C2, R32, and $P3_221$ space groups and diffracted X-rays to 3.2 Å (14-mer), 2.55 Å (18-mer), and 2.4 Å (20-mer) resolutions (Table 1). X-ray diffraction data of the native and selenomethionine substituted 18-mer crystals were collected from an in-house X-ray source to 3.1 Å resolution. The Se structure was solved by the single isomorphous replacement (SIR) method using the program SOLVE (Terwilliger and Berendzen, 1999) (Table S2). The experimental maps were clear (Figure S2), and the complete model was readily traceable. The resulting model was used in molecular replacement to solve the higher resolution structure of the 18-mer complex as well as the 14- and 20-mer structures. The three crystal structures are refined (Figure 1), and the data collection and refinement statistics are shown in Table 1.

Structure of Hs-RNase HC

The RNase HC molecules from the 18-mer and 20-mer crystals can be superimposed including all Cα atoms to a root-mean-square deviation (rmsd) of 0.4 Å and are thus considered identical. The only significant differences among Hs-RNase HC structures are observed in two loops (residues 263–267 and 153–157) (Figure 1A). The central element of Hs-RNase HC is a mixed β sheet comprising five strands (Figure 1). On one side of the β sheet there are four α helices (A, B, C, and D). The fifth and last α-helix (E) is located on the other side of the β sheet. As predicted, D145 located in the middle of strand 1, E186 in helix A, D210 at the end of strand 4, and D274 in helix E form the active site (Figures 2A and 2B).

The overall folds of RNases H from *E. coli*, *B. halodurans*, HIV, human, and that of the recently solved Moloney murine leukemia virus (Mo-MLV) protein (Lim et al., 2006) are very similar. The central β sheet and helices A, B, and D are present in all RNase H catalytic domains. Human, Mo-MLV, and *E. coli* RNases H differ from the other two by possessing the basic protrusion consisting of helix C and the following loop (Figure 2A). When the human and *E. coli* proteins are superimposed, the rmsd for 109 pairs of Cα atoms within the secondary structural elements is 1.3 Å, and the rmsd for all 146 Cα pairs is 2.6 Å. The largest deviations occur in the basic protrusion region (2.5–6 Å), probably due to the substrate binding by Hs-RNase HC. With only 34% sequence identity, human and *E. coli* RNases H are remarkably similar in their three-dimensional structures (Figure 2C).

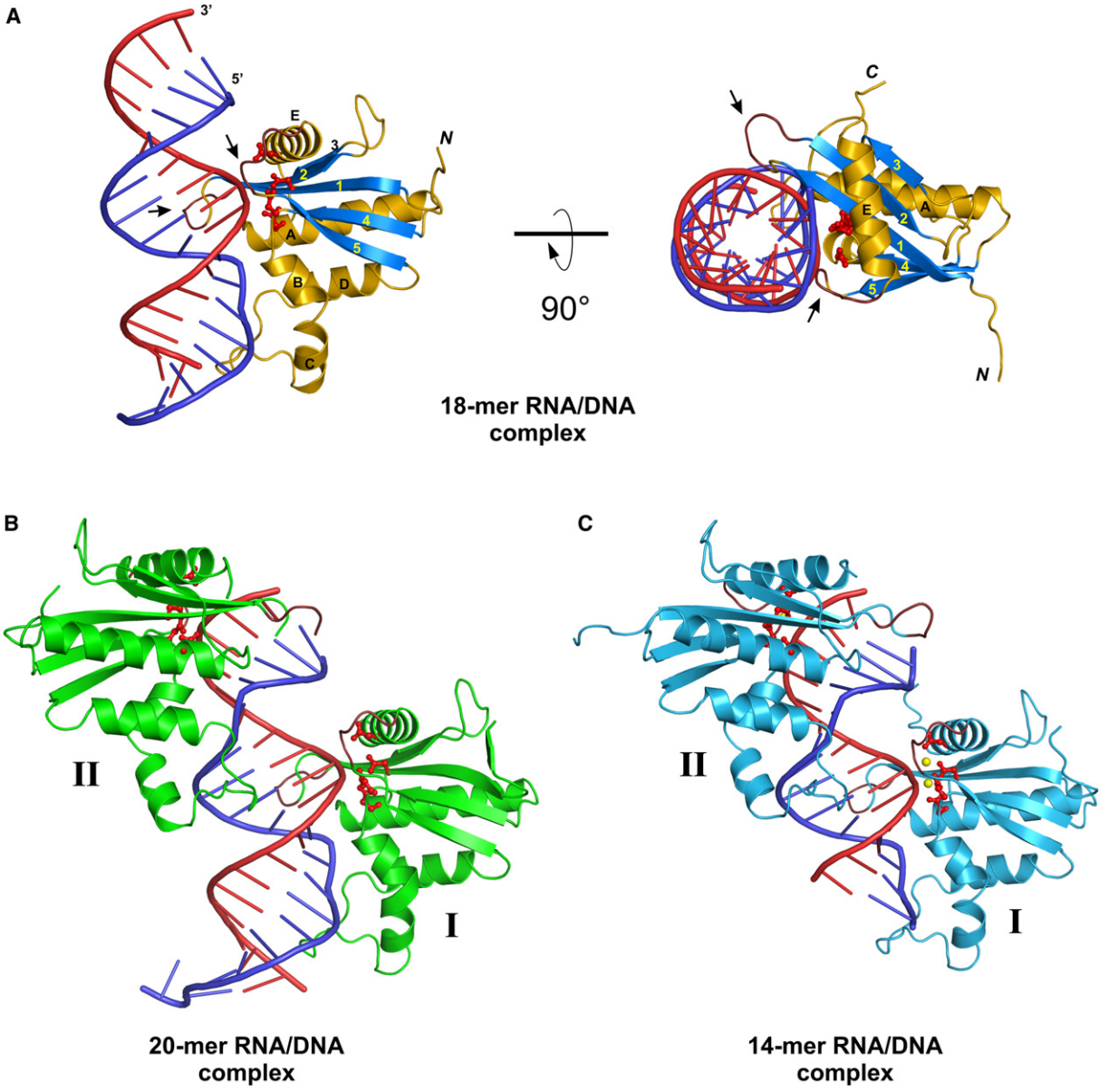

Figure 1. Crystal Structures of Hs-RNase HC Complexed with RNA/DNA Hybrids

(A) 18-mer RNA/DNA complex. The protein is shown in a gold and blue ribbon diagram with secondary structure elements labeled. The substrate is shown in red (RNA) and blue (DNA) tube representations. The active site residues are shown in red ball-and-stick model. Loops whose conformation varies among Hs-RNase HC structures are in brown and are indicated with arrows.

(B and C) (B) 20-mer and (C) 14-mer RNA/DNA complexes. In the 20-mer complex, the base pair at one end of the substrate is unpaired, and both nucleotides are flipped out with the electron density visible only for one base.

Substrate Recognition

An Hs-RNase HC molecule interacts with 11 bp of the 18-mer RNA/DNA hybrid (Figures 1 and 3). Except for the contacts formed by the tip of the basic protrusion, the majority of the enzyme-substrate interactions occur along the minor groove of the hybrid. The protein surface contains two grooves separated by a ridge composed of highly conserved N151, N182, and Q183 (Figure 2A). The minor groove of the RNA/DNA hybrid straddles the ridge, and the RNA and DNA backbones fit in the grooves (Figure 3B).

The RNA strand is in the regular A form with C3′-endo sugar puckers as expected. The active site is located in the RNA-binding groove, which interacts with the 2′-OH groups of four consecutive ribonucleotides, two on each side of the scissile phosphate (Figure 3A). These contacts

Table 1. X-Ray Data Collection and Refinement Statistics

Data Collection and Refinement	Native 14-Mer RNA/DNA Complex	Native 18-Mer RNA/DNA Complex	SeMet 20-Mer RNA/DNA Complex
Radiation source	Advanced Photon Source, ID-22		
Wavelength (Å)	0.9793	1.0	1.0
Space group	C2	R3 2	$P3_2$ 2 1
Unit cell a, b, c (Å)	151.1, 176.3, 125.8	158.6, 158.6, 142.0	110.0, 110.0 67.2
α, β, γ (°)	90.0, 90.2, 90.0	90, 90, 120	90, 90, 120
Resolution range (Å)[a]	30 – 3.2	30 – 2.55	40 – 2.4
	(3.3 – 3.2)	(2.64 – 2.55)	(2.49 – 2.40)
Completeness (%)[a]	95.8 (74.1)	97.5 (83.5)	95.4 (69.1)
R_{merge}[a,b]	13.9 (41.7)	7.4 (45.6)	6.0 (45.2)
I/σ(I)[a]	14.7 (3.2)	38.7 (4.1)	35.8 (2.7)
Unique reflection	50322 (1752)	21164 (2085)	16949 (1680)
Nonhydrogen atoms refined	16241	2112	3246
R value[c]	21.2	18.8	20.8
R_{free}[d]	26.5	21.6	25.5
Rmsd bond length (Å)	0.0076	0.013	0.013
Rmsd bond angle (°)	1.47	1.90	1.75
Average B value (Å^2)	62.4	43.4	59.6
ϕ, ψ distribution (%)[e]	72.5, 23.5, 2.9, 1.0	89.8, 8.6, 1.6, 0	88.3, 10.0, 1.7, 0

[a] Data of the highest-resolution shell are shown in parenthesis.
[b] $R_{merge} = \sum h \sum i |Ihi - <Ih>| / \sum <Ih>$, where Ihi is the intensity of the ith observation of reflection h and <Ih> is the average intensity of redundant measurements of the h reflections.
[c] R value = $\sum ||F_o| - |F_c|| / \sum |F_o|$, where F_o and F_c are the observed and calculated structure factor amplitudes.
[d] R_{free} is monitored with the number of reflections in parenthesis excluded from refinement.
[e] Residues in the most favored, additionally allowed, generously allowed, and disallowed regions of the Ramachandran plot.

are mediated by the side chain of E186 (helix A) and the backbone atoms of C148, S150, and N151 (at the end of strand 1) and M212 (helix B). The RNA strands complexed with human and *B. halodurans* RNase H superimpose well (Figure S3), and the overall mechanism for RNA strand recognition is thus conserved.

Hs-RNase HC interacts with seven nucleotides of the DNA strand. The most prominent DNA-protein contacts are formed by R179, T181, and N240 with the phosphate two base pairs from the scissile bond (Figure 3D). A similar phosphate-binding pocket was first observed in the Bh-RNase H structures (Nowotny et al., 2005). The pockets are spatially conserved but share only one conserved residue, T181 in Hs-RNase H and T104 in Bh-RNase H (Figure S3). To place the phosphate in the pocket requires large distortions of the backbone torsion angles (gamma and alpha) by ~150° from the ideal values. Only DNA can assume such a conformation. Chemical modifications of a single deoxyribonucleotide that result in an A form sugar pucker prevent cleavage of the opposing ribonucleotide and two ribonucleotides downstream by Hs-RNase H (Lima et al., 2004), which confirms the importance of the phosphate-binding pocket in substrate recognition and specification for B form DNA.

The second DNA-binding site is a channel formed by W221, W225, and S233 in the basic protrusion (Figure 3E). The DNA backbone fits snugly into this channel, making van der Waals contacts and hydrogen bonds. When an RNA strand is modeled into this channel based on the positions of the phosphosugar backbone, a 2′-OH group clashes with the indole ring of W221. Interestingly, the DNA strand is mainly B-like (between C2′-endo and O4′-endo) except for the deoxynucleotide in the DNA-binding channel, which is between A and B form (C4′-exo). As a result of the distorted DNA strand, the minor groove width of the RNA/DNA duplex varies from 7 Å at the phosphate-binding pocket to 11.7 Å at the DNA-binding channel (Figure 3C). Such variations are not observed in the complexes with Bh-RNase HC without the basic protrusion. We conclude that Hs-RNase H most likely recognizes the DNA strand by the absence of 2′-OH as required by the DNA-binding channel and by the flexible B form conformation as imposed by the phosphate-binding pocket.

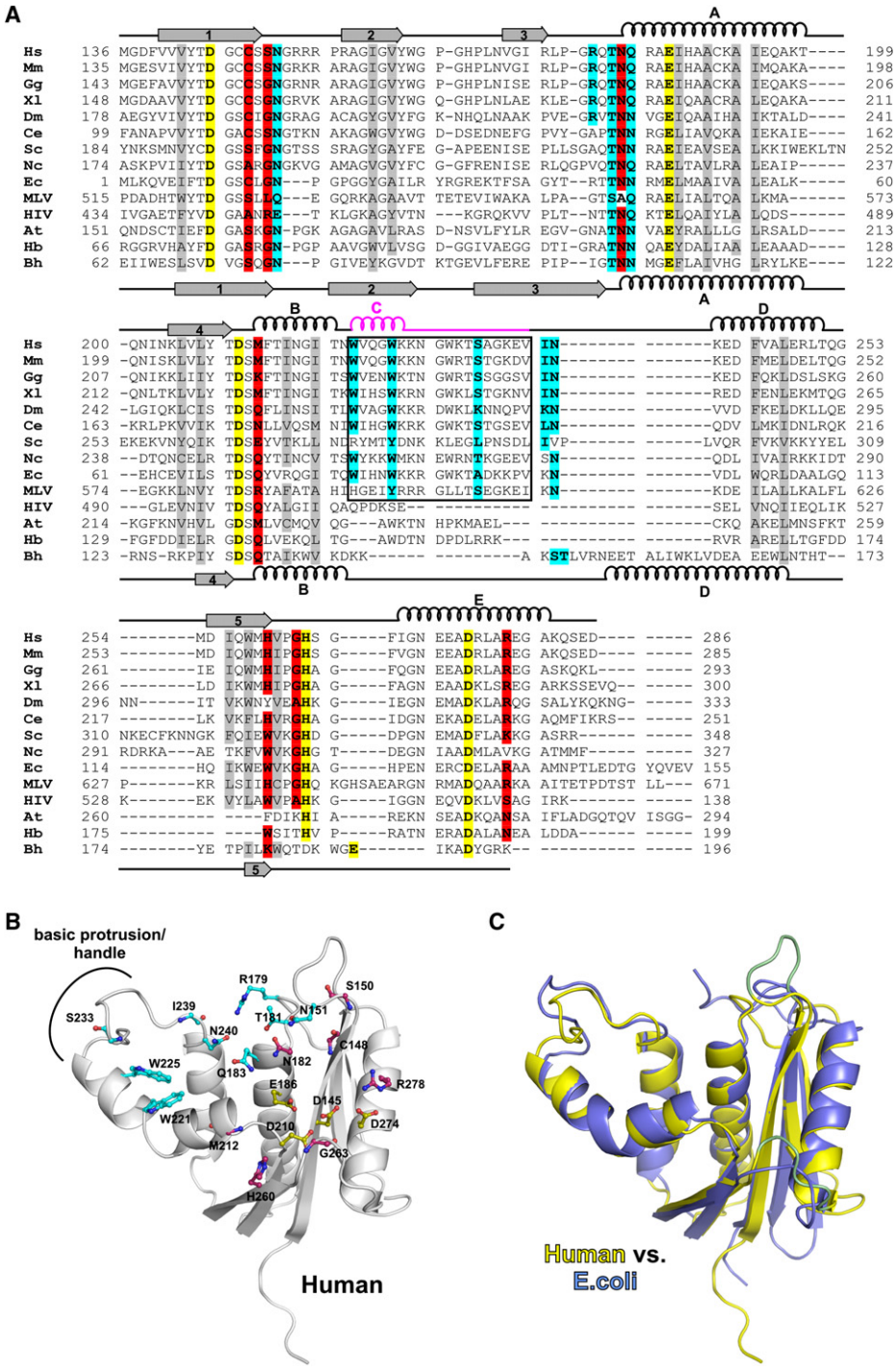

Figure 2. Comparison of RNases H

(A) Sequence alignment of catalytic domains of multiple RNases H. Conserved residues in the active site are highlighted in yellow, interacting with the RNA strand in red and interacting with the DNA in cyan. Conserved hydrophobic core residues are highlighted in gray. Secondary structures of Hs-RNase HC and Bh-RNase HC are indicated. The basic protrusion region is colored in pink and its sequence boxed. Hs, human; Mm, mouse; Gg, chicken; Xl, *X. leavis*; Dm, *D. melanogaster*; Ce, *C. elegans* (RNase H1.0); Sc, *S. cerevisae*; Nc, *N. crassa* (hypothetical protein); Ec, *E. coli*; MLV, Moloney murine leukemia virus RT; HIV, human immunodeficiency virus RT; At, *A. thaliana* (putative RNase H1); Hb, *Halobacterium* sp. NRC-1; Bh, *B. halodurans*.

(B) Ribbon representation of human RNase H with residues involved in catalysis (yellow), RNA binding (magenta), and DNA binding (cyan) shown in ball-and-stick model. For protein backbone-mediated interactions, only the backbone atoms of the residues involved are shown.

(C) Superposition of human (yellow) and *E. coli* (blue) RNases H. Mobile loops are in light green.

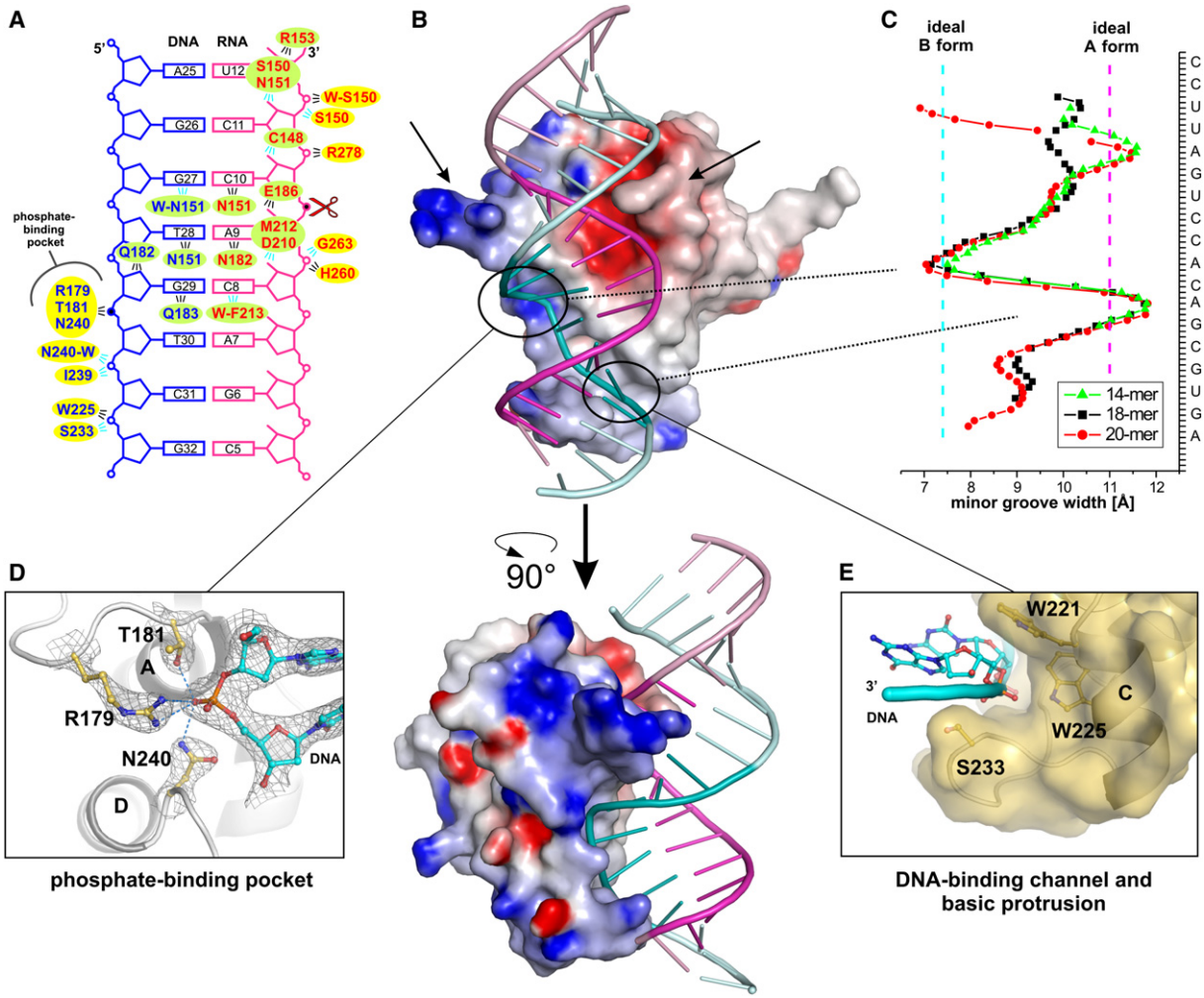

Figure 3. Substrate Binding by Hs-RNase HC

(A) Diagram of the protein-nucleic acid interactions. Yellow highlight represents residues interacting with the backbone of the substrate and green highlight for interacting with sugars and bases. Cyan and black lines indicate interactions mediated by the backbone and side chains of the protein, respectively. Water-mediated interactions are indicated by "–W."

(B) Orthogonal views of the surface potential representation of Hs-RNase HC and the 18-mer RNA/DNA hybrid in the tube-and-stick model (RNA, magenta/pink; DNA, cyan). The nucleotides interacting with the protein are highlighted in darker color. Arrows indicate the position of the mobile loops.

(C) Plot of the minor groove width of the 14-, 18-, and 20-mer RNA/DNA hybrid in complex with Hs-RNase HC D210N. The minor groove widths of ideal A and B form helices are indicated.

(D) DNA binding in the phosphate-binding pocket. A $2F_o - F_c$ simulated annealing omit map contoured at 1.5 σ is superimposed over the model.

(E) The interaction of the substrate with the DNA-binding channel in basic protrusion.

Substrate-Binding and Cleavage Specificity

E. coli RNase H can bind not only RNA/DNA but also dsRNA, which acts as a competitive inhibitor with ~1 μM affinity (Lima and Crooke, 1997). Such inhibition has also been reported for the full-length Hs-RNase H, in which both the catalytic domain and the N-terminal RHBD may contribute to the dsRNA binding (Wu et al., 1999). To examine the substrate-binding specificity of the catalytic domain of Hs-RNase H, electrophoretic mobility shift assays (EMSAs) and sedimentation equilibrium experiments were performed on the D210N mutant Hs-RNase HC and a 12-mer RNA/DNA hybrid or dsRNA and dsDNA of the corresponding sequence. EMSA assays showed that Hs-RNase HC binds both RNA/DNA and dsRNA (Figure S4). Sedimentation equilibrium experiments showed that Hs-RNase HC and the RNA/DNA hybrid formed complete 1:1 complexes at loading concentrations as low as 0.6–0.7 μM, and the exact Kd is too low to be determined (Figure 4A and Figure S5). In the case of dsRNA and dsDNA, Kd values for the reversible 1:1 interaction were determined to be 3.1 ± 0.4 μM and 29 ± 4 μM, respectively (Figure 4A and Figure S5). Hs-RNase HC thus binds dsRNA but prefers RNA/DNA hybrids. The interaction with the dsRNA can occur between one RNA strand and

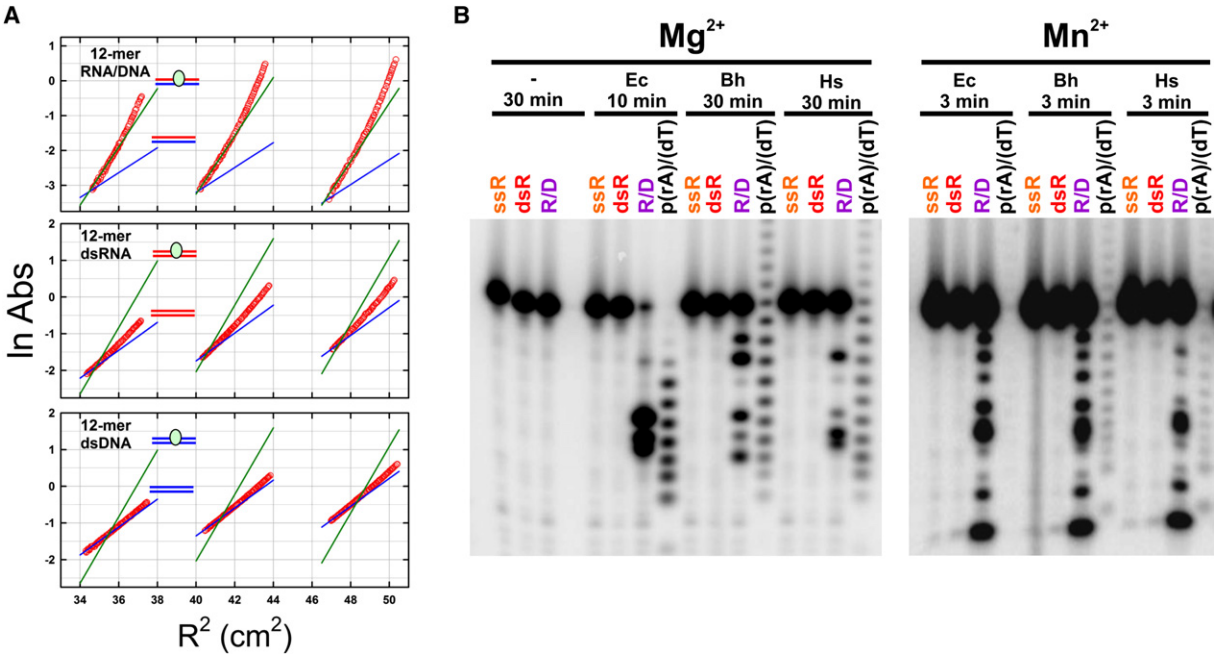

Figure 4. Binding and Cleavage Specificity of Hs-RNase HC

(A) Sedimentation equilibrium profiles at 21 krpm for Hs-RNase H (D210N) with the 12-mer RNA/DNA at the nominal loading of A_{230} of 0.22 (left), 0.48 (center), and 0.82 (right) and sedimentation equilibrium profiles at 22 krpm for Hs-RNase H (D210N) with the 12-mer dsRNA and dsDNA at the nominal loading of A_{280} of 0.3 (left), 0.6 (center), and 0.9 (right). The solid blue lines show the slope expected for the free duplex nucleic acid, whereas the solid green lines show the slope expected for the 1:1 protein:nucleic acid complex. Complete data analyses are found in the Supplemental Data.

(B) Hydrolysis assays of *E. coli* RNase H (Ec), *B. halodurans* RNase HC (Bh), and human RNase HC (Hs). 12-mer ssRNA, dsRNA, RNA/DNA of corresponding sequences, or uniformly labeled poly(rA)/poly(dT) were digested for indicated time in the presence of 5 mM $MgCl_2$ or 10 mM $MnCl_2$, and the products were resolved on denaturing urea-PAGE.

the RNA interface. The second RNA strand obviously cannot fit in the phosphate-binding pocket or the DNA channel, but it may interact with positively charged residues, for example, in the basic protrusion. This suboptimal binding would explain the reduced affinity for dsRNA.

To determine whether *E. coli*, *B. halodurans*, and human RNases HC can cleave dsRNA as well as RNA/DNA hybrids, digestion experiments were performed in the presence of 5 mM $MgCl_2$ (Figure 4B). Only RNA in the 12-mer RNA/DNA was cleaved, and ssRNA and dsRNA of the corresponding sequence remained intact. Cleavage assays were also performed in the presence of Mn^{2+}, since it supports dsRNA cleavage by HIV and Mo-MLV RTs (Ben-Artzi et al., 1992; Blain and Goff, 1993). In our assays, Mn^{2+} does broaden the cleavage pattern and seemingly reduces the cleavage stringency. But it fails to enable any of the three RNases H to cleave dsRNA. Despite dsRNA binding with micromolar affinity, cleavage by the cellular RNases H is highly specific for RNA/DNA hybrids.

An inspection of the surface potential of Hs-RNase HC reveals that the most positively charged areas are outside of the substrate interface—for instance, the conserved K226 and K227 in the basic protrusion and R153 and R154 between strand 1 and 2 (Figure 3B). Notably, these residues are located adjacent to the substrate interface, and R153 and R154 are on one of the two mobile loops in Hs-RNase HC (Figure 1). These positively charged areas may facilitate initial nonspecific interactions with nucleic acids and promote the formation of specific enzyme-substrate complexes. Specific binding of the RNA/DNA hybrid that leads to catalysis must not solely rely on the electrostatic attraction but rather depend on the surface complementarity and the snug fitting of the DNA strand.

Two-Metal Ion Catalysis

The crystals of Hs-RNase HC 18-mer complexes were grown in high ionic strength without divalent metal ions. Although Mg^{2+} and Mn^{2+} soaking experiments were performed, no additional electron densities corresponding to the divalent metal ions were detected. The 14-mer complex crystals, however, were grown in the presence of 0.2 M calcium acetate and allowed us to analyze the metal binding in the active site. There are six complexes of two protein molecules bound to one RNA/DNA hybrid in each asymmetric unit, and 11 independent protein-substrate interfaces were in effect observed (Figure S6). Even at the resolution of 3.2 Å, the Ca^{2+} ions were readily identified in the 11 active sites (Figures 5A and 5B). Depending on the crystal lattice contacts, a spectrum of scissile phosphate location and number of Ca^{2+} ions in each active site was observed. On one end of the spectrum was the "productive complex," in which two Ca^{2+} ions

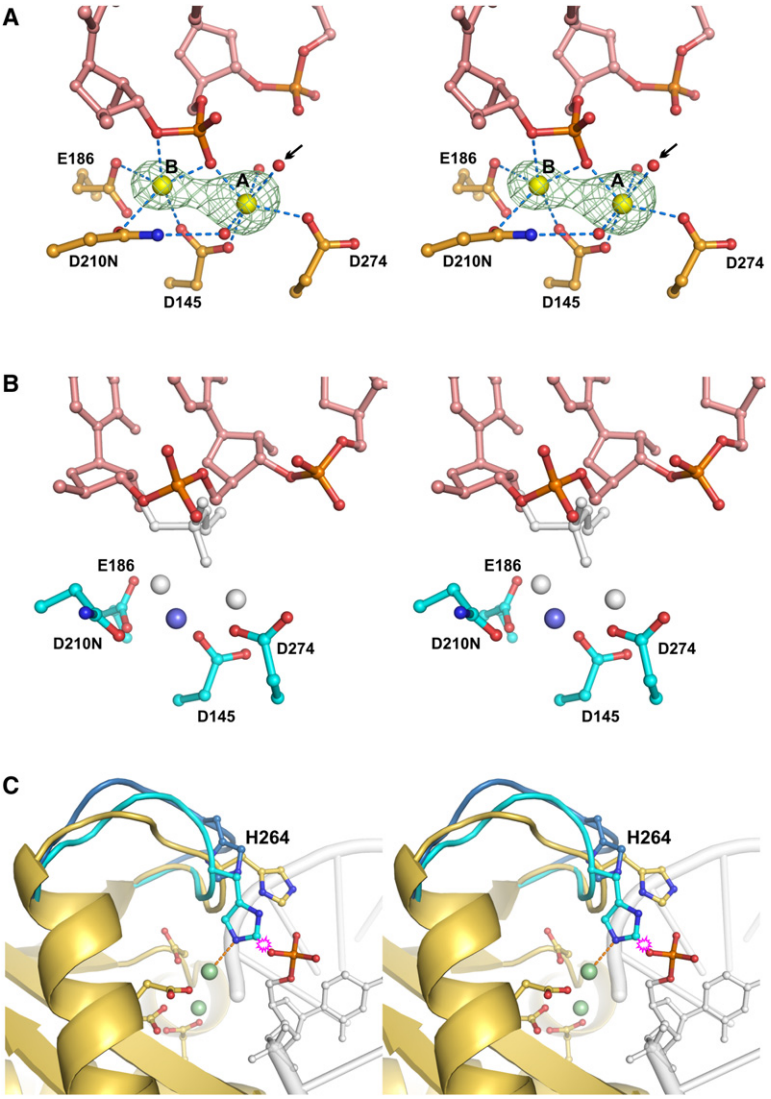

Figure 5. The Active Site of Hs-RNase HC D210N

(A) Stereo view of the "productive" subunit from the complex with 14-mer RNA/DNA. Active site residues are shown in orange, the RNA in pink and Ca^{2+} ions as yellow spheres. An F_o-F_c omit map for calcium ions contoured at 7 σ is shown in green and metal ion coordination is represented by blue dashed lines. Water molecules are shown as small red spheres. The attacking nucleophile is indicated with an arrow.

(B) Stereo view of the "nonproductive" subunit of the 14-mer RNA/DNA complex with the displaced scissile phosphate. The active site residues are shown in cyan and the calcium ion as a blue sphere. The scissile phosphate and calcium ions from superimposed "productive" subunit are shown in light gray as reference.

(C) Conformation of histidine 264 (stereo view). Superimposed protein structures from the complex of Hs-RNase HC with 18-mer (gold) and 20-mer RNA/DNA (blue, two subunits) are shown in ribbon diagrams and histidine 264 and active site residues shown as ball-and-stick models. 5′-phosphorylated product from the Bh-RNase HC complex superimposed on human complex structures is shown in gray with phosphate group in color. Magnesium ions from the product complex are shown as light green spheres. The collision between the phosphate group and histidine residue is shown in purple and a potential contact between histidine and Mg^{2+} ion as orange line.

were found in the active site approximately occupying the canonical A and B positions (Figure 5A). Metal ion B is coordinated by five ligands: active site residues D145, E186, and D210(N) and pro-S_p nonbridging and 3′ (leaving group) oxygen atoms of the scissile phosphate. Metal ion A is coordinated in octahedral configuration by D145 and D274 and pro-S_p nonbridging oxygen of the scissile phosphate. Such active sites are superimposable with that of *Bh*-RNase HC, including the scissile phosphate (Nowotny et al., 2005). Therefore, it is safe to assume that human RNase H uses the same two-metal ion mechanism for catalysis (Steitz and Steitz, 1993; Yang et al., 2006).

On the other end of the spectrum was the "nonproductive complex," where the scissile phosphate was displaced from the active site due to the disruptive crystal packing. In this case, only one metal ion, ~2.5 Å from the canonical B and A sites, was observed (Figure 5B). The different formations of the active site illustrate an important property of the two-metal ion mechanism, namely that productive metal ion binding is substrate dependent. In apo structures, one metal ion is most often observed in the RNase H active site at a location away from the canonical A or B site (for an example, see Katayanagi et al., 1993). The nonproductive complex confirms that without the proper positioning of the scissile phosphate, neither the A nor the B site is occupied. Conversely, without A and B metal ions properly positioned in the active site, the scissile phosphate cannot be positioned correctly in the active site for RNA hydrolysis (Yang et al., 2006).

A histidine C-terminal to the active site carboxylates is conserved in many RNases H (H124 in *E. coli*, H539 in HIV RT, and H264 in human) (Figure 2A) and is required for the full activity (Oda et al., 1993; Tisdale et al., 1991). H264 in human enzyme is located between strand 5 and helix E on a mobile loop flanking the active site (Figure 5C). E188 in Bh-RNase H is located on a similar loop after strand 5, and it also strongly influences the catalytic

efficiency (Nowotny et al., 2005). The proposed role of E188 is to promote the dissociation of the reaction product (Nowotny and Yang, 2006). When human RNase HC is superimposed onto the Bh-RNase HC (E188A)-product complex, the imidazole ring of H264 clashes with the cleaved 5′-phosphate. Thus, it appears that H264 together with the mobile loop may facilitate product release by dislodging the 5′-phosphate.

Modeling an RNA/DNA Hybrid in the RNase H Active Site of HIV RT

HIV RT is a heterodimer composed of p66 and p51 subunits. p66 has an elongated shape and contains both the polymerase and RNase H active sites ~70 Å apart. p51 is thought to mainly play a structural role. The two active sites are connected by a long cleft formed between p66 and p51. Crystal structures of HIV RT (Kohlstaedt et al., 1992) and its complexes with dsDNA (Huang et al., 1998) or RNA/DNA hybrid (Sarafianos et al., 2001) have been determined. Both the dsDNA and RNA/DNA hybrid in the cocrystal structures are poised for primer extension by the polymerase domain, and they extend to the RNase H domain but miss its active site by ~4 Å. Thus, how HIV RNase H binds and cleaves its substrate remains unknown.

Cleavage of RNA/DNA hybrid by HIV RT RNase H is most efficient at ~18 bp from the 3′ end of DNA during reverse transcription or ~18 bp from the 5′ end of a recessed RNA (as during removal of remaining RNA fragments) (Gopalakrishnan et al., 1992; Palaniappan et al., 1996). Oriented by the 3′ and 5′ overhangs, the 18 bp duplex must lie between the polymerase and RNase H active sites in the substrate-binding cleft. This hypothesis is supported by several lines of evidence. First, cleavages and primer extension can occur from a single binding event (DeStefano et al., 1991; Gopalakrishnan et al., 1992). Second, after the extension of the primer by several nucleotides, the RNase H cleavage sites move accordingly and remain at a fixed distance from the 3′ end of the primer (Furfine and Reardon, 1991; Gopalakrishnan et al., 1992). Finally, the intact polymerase domain of p66 is necessary for the efficient substrate binding and cleavage by RNase H (Gao et al., 1998). HIV RT can also carry out internal cleavages of long RNA/DNA hybrids (Schultz et al., 2004). The double-stranded substrate beyond 18 bp most likely exits from the polymerase in the gap between the thumb and finger domains.

A comparison of the enzyme-substrate complex structures of human and *B. halodurans* RNases H (Figure S3) leads to the identification of conserved elements for substrate binding. The active site and surrounding area define the RNA interface, and the spatially conserved phosphate-binding pocket defines a DNA-binding site. The active site and the RNA interface are conserved in HIV RNase H (Figure 6A). The location of the phosphate-binding pocket is also conserved in HIV RT, but it is composed of two residues (T473 and K476) instead of three as in Hs-RNase HC (R179, T181, and N240) (Figure S7). We thus predict that substrate binding in the RNA interface and the phosphate-binding pocket will be conserved in HIV RNase H. However, perhaps due to the absence of a third ligand in the phosphate-binding pocket, HIV RNase H domain alone is ineffective and requires the rest of RT for Mg^{2+}-dependent and efficient RNA degradation (Hostomsky et al., 1991).

When the Hs-RNase HC-RNA/DNA hybrid complex structure was superimposed on the RNase H domain of HIV RT (Protein Data Bank [PDB], 1HYS) using conserved secondary structure elements, 6 bp of the RNA/DNA hybrid readily fit onto HIV RT, 3 bp on each side of the RNase H active site (Figure 6C). With a slight adjustment (Figure 6F), two more nucleotides of the DNA strand beyond the phosphate-binding pocket can interact with the "primer grip" (residues G359, A360, and H361 in the p66 subunit) (Sarafianos et al., 2001), which replaces the basic protrusion of Hs-RNase HC. Beyond the primer grip, the RNA/DNA hybrid has to bend and deviate from the trajectory observed in the complex with Hs-RNase HC to avoid clashes with the p51 subunit (Figure 6F). Different substrate orientation beyond the phosphate-binding pocket has also been observed between human and *B. halodurans* RNase H (Figure 6B and Figure S3).

The helical axis of the hybrid that fits in the RNase H active site is at an ~20° angle and displaced by 3.5 Å from the helical axis of the RNA/DNA duplex extended from the polymerase active site (PDB, 1HYS) (Figures 6D and 6E). The DNA backbones of the two hybrid duplexes do intersect at the phosphate-binding pocket and can be connected to form a continuous strand. When this connection is made, however, the RNA strands are separated by a gap of 17 Å and cannot be joined (Figure 6E). The misalignment is unlikely to be alleviated by movement of the RNase H domain, as it is an integral part of HIV RT and relatively immobile among the HIV RT structures reported to date. This is very different from Mo-MLV RT, which contains a 32-residue linker between the RNase H and polymerase domains and a mobile RNase H as a result (Das and Georgiadis, 2004). In conjunction with such mobility, the Mo-MLV RNase H domain has the basic protrusion for substrate binding.

An RNA/DNA hybrid, however, can be accommodated in the RNase H active site and extended to the polymerase domain if the 18-mer duplex is bent in the middle by a minimal angle of ~35° (Figure 6F). In the HIV RT cocrystal structures, the substrate-binding cleft is predominantly positively charged, and its wide midsection formed between p51 and the connection domain of p66 scarcely interacts with the polymerase substrate (Figures 6D and 6E). This midsection provides ample space to accommodate and form favorable interactions with the proposed bent RNA/DNA hybrid (Figure 6F). Two residues in particular are predicted to interact with the bent RNA/DNA—R83 and W266 from p51 subunit. Interestingly, mutation of W266 in p51 inhibits the RNase H activity of HIV RT (Gao et al., 1998). To allow an RNA/DNA hybrid longer than 18 bp to exit from HIV RT between the finger and

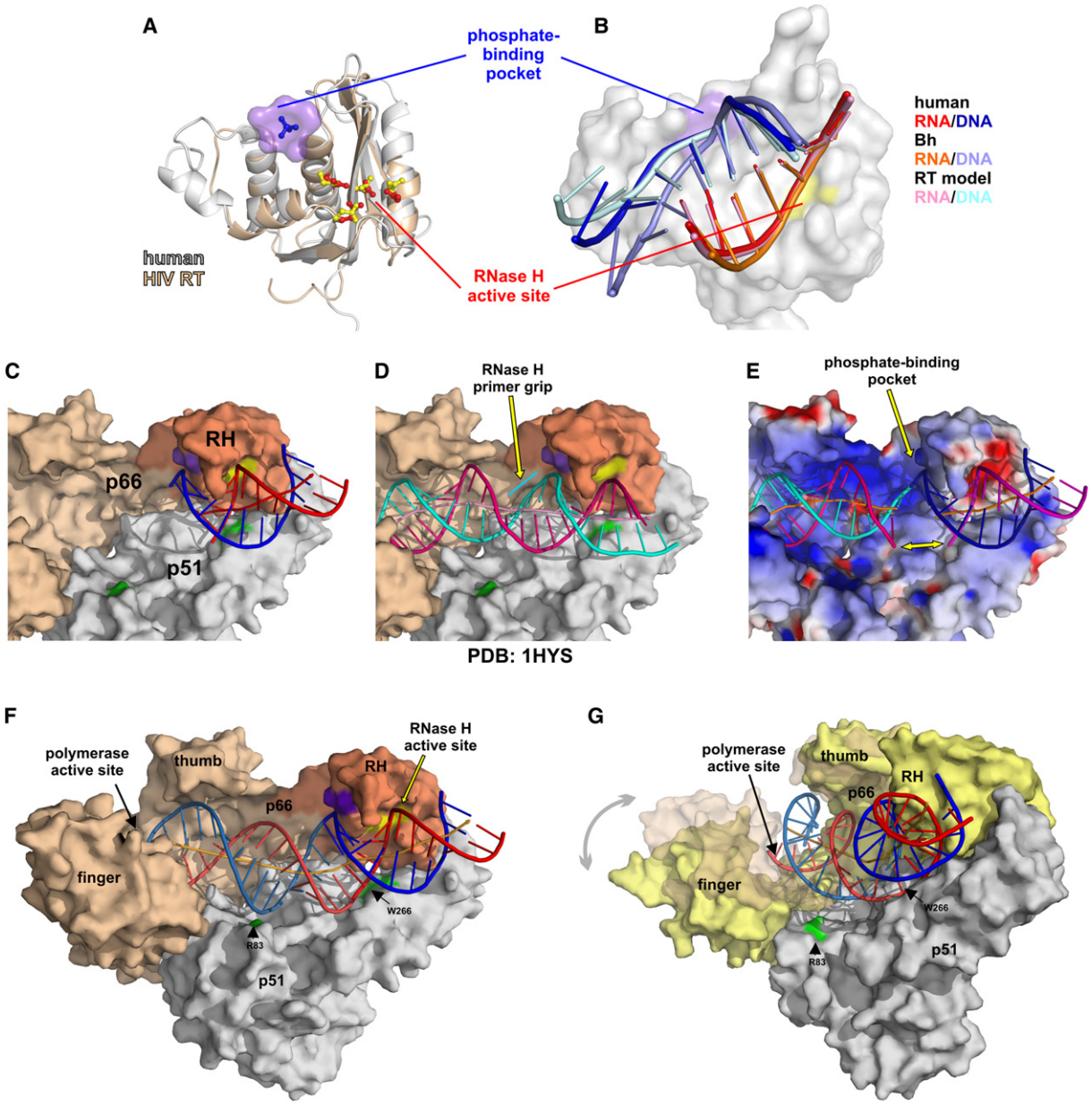

Figure 6. Model of RNase H—Substrate Complex of HIV RT

(A) Superposition of human and HIV RNases H. Active site residues are shown in yellow (HIV) and red (human). Surface of the phosphate-binding pocket and the interacting DNA phosphate group are shown.

(B) Comparison of the substrate orientation after superposition of Hs-RNase HC D210N complexed with the 18-mer RNA/DNA, Bh-RNase HC D132N in complex with 12-mer RNA/DNA (PDB, 1ZBI), and HIV RT model.

(C) Docking the RNA/DNA hybrid from the Hs-RNase HC structure onto HIV RT. After superposition of the RNase H domain, the substrate from the human structure is shown in red (RNA) and blue (DNA) with the helical axis in red, and the HIV RT heterodimer is shown as molecular surface with the active site (yellow) and phosphate-binding pocket (purple) indicated.

(D) The cocrystal structure of HIV RT and RNA/DNA hybrid (PDB, 1HYS). The RNA is in pink and the DNA in cyan.

(E) The RNA/DNA hybrid extended from the polymerase active site (PDB, 1HYS) cannot be joined with the modeled hybrid in the RNase H active site. The gap in the RNA strand is indicated with a yellow arrow. The surface of HIV RT is colored according to its electrostatic potential (blue, positive; red, negative), and the wide midsection of the substrate-binding cleft is highly positively charged.

(F) Hypothetical model of HIV RT in complex with RNA/DNA hybrid interacting with the polymerase domain but engaged only at the active site of RNase H (RNA in red and DNA in blue). R83 and W266 potentially mediating the contacts between p51 and the bent substrate are highlighted in green.

(G) Side view of the HIV RT model. The surface of RT from complex crystal structure (PDB, 1HYS) is shown in light brown (p66, transparent) and white (p51). Superimposed p66 subunit from the PDB, 2HNY, structure is shown in yellow. The movement of the finger domain is indicated with an arrow.

thumb domains, the finger needs to adopt an open conformation (as observed in PDB, 2HNY, and other structures in the same space group) (Figure 6G), and the bend in the duplex may be larger than 35°.

A bent RNA/DNA substrate is most probably essential for cleavage by HIV RT, and the resistance of the polypurine tract (PPT) to cleavage may result from its inability to adopt a bent conformation. The PPT contains an A tract followed by a G tract. A tracts are known for being stiff and straight, while an rA/rG junction is deformable (Kopka et al., 2003). The cleavage of PPT by HIV RT occurs 4–6 bp from the rA/rG junction (Rausch et al., 2003). Also, when dC and dT analogs that increase the duplex flexibility were introduced into the PPT, its cleavage by HIV RT was repositioned to ~4 bp from the modification site (Rausch et al., 2003). The observed cleavage site with regards to the flexible point in PPT matches our HIV RT model with an RNA/DNA substrate in the RNase H active site (Figure 6F).

The bent duplex extended from the RNase H active site is displaced from the polymerase active site by ~7 Å, and the 18th base pair from the scissile phosphate is the last one that can be modeled without clashes with the polymerase domain. A wealth of biochemical data have documented that the polymerase and RNase H activities of HIV RT, although located on a single polypeptide chain, do not simultaneously act on the substrate. First, mixing mutant HIV RTs deficient in either polymerase or RNase H fully restores reverse transcription in vitro (Shaw-Reid et al., 2005). Second, the RT molecule that catalyzes RNA-dependent DNA synthesis does not processively degrade the resulting hybrid (DeStefano et al., 1991), and the polymerization reaction is 7- to 10-fold faster than the degradation by RNase H (Kati et al., 1992). Third, stabilization of an RNA/DNA hybrid in the polymerase active site of HIV RT by a correct incoming nucleotide inhibits the RNase H activity (Furfine and Reardon, 1991). Fourth, RNase H cleavage appears to occur when polymerase pauses (Purohit et al., 2007), and nonnucleotide RT inhibitors (NNRTIs) that impede DNA polymerization often enhance the RNase H activity (Shaw-Reid et al., 2005). We therefore propose that the polymerase and RNase H activities of HIV RT are mutually exclusive and that a substrate can interact with one active site at a time.

Target Sites for Anti-HIV RT Drug Development

In spite of the highly conserved active site, the differences between human and HIV RNases H in substrate binding provide grounds for designing inhibitors that may specifically target the viral enzyme. The phosphate-biding pocket, in which significant differences are observed between human and HIV RNases H (Figure S7), presents one prime target. In addition to the different amino acid composition, the pocket in Hs-RNase HC is complete, but in HIV RT it misses a part of the rim and is connected to a hydrophobic cleft. This extended and partially hydrophobic phosphate-binding pocket may be targeted by a small molecule.

The midsection of the substrate-binding cleft, which, based on our modeling exercise, accommodates the bent substrate, is another potential drug target. Blockage of RNA/DNA substrate from switching between the polymerase and RNase H active sites of HIV RT may effectively inhibit reverse transcription and viral infection. A small molecule binding in this region and inhibiting substrate conformational changes must interact with both the protein and the nucleic acid substrate. Thus, identification of lead compounds requires screenings when one of the active sites is engaged in catalysis.

EXPERIMENTAL PROCEDURES

Protein Preparation

Both native and selenomethionine-labeled Hs-RNase HC D210N (residues 136–286) was expressed in *E. coli* from pET15-based vector and purified on Ni column and Mono S. For detailed protocol, see the Supplemental Data.

Crystallization

RNA oligonucleotides were purchased from Dharmacon and DNA oligos from IDT (see Table S1 for sequences). Oligo RNAs were purified using urea-PAGE. The RNAs were eluted from gel fragments in the buffer containing 10 mM Tris (pH 8.0), 300 mM NaCl, and 5 mM EDTA. Oligo DNAs (with trityl group on) were purified by HPLC using a reverse-phase R3 column (Applied Biosystems) and detritylated.

Native or SeMet Hs-RNase HC D210N (~0.3 mg/ml) was mixed with the RNA/DNA hybrids at 1.8:1 molar ratio. The complexes were concentrated in YM-10 centricons (Amicon) to 4.5–6.5 mg/ml. The concentrated complexes were mixed with the reservoir solution at equal volume and crystallized by the hanging drop vapor diffusion method at 21°C. The 14-mer complex crystals were obtained with 12% isopropanol, 0.2 M calcium acetate, and 0.1 M MES (pH 6.0) with 0.1 M LiCl added to the crystallization drops. For data collection, the crystals were transferred stepwise to cryoprotecting solutions with decreasing isopropanol concentration and increasing MPD and glycerol concentrations. The final solution contained 20% MPD, 5% glycerol, 0.2 M calcium acetate, 0.1 M MES (pH 6.0), and 0.1 M LiCl. The crystals were flash cooled in liquid nitrogen. The 18-mer complex crystals were obtained with 1.5 M ammonium sulfate and 0.1 M Na citrate (pH 5.6). ATP (20 mM) or 3% 1,6-diaminohexane was added to the crystallization drop to obtain crystals of improved size. The cryosolution contained 2.5 M ammonium sulfate, 0.1 Na citrate (pH 5.6), and 20% glycerol. The 20-mer crystals could only be grown with the SeMet protein. The well solution contained 15% PEG 3350, 0.1 M $LiSO_4$, and 0.1 M Tris (pH 8.5), and for cryo protection 25% PEG 3350, 0.1M $Li2SO_4$, 0.1 M Tris (pH 8.5), and 10% ethylene glycol were used.

Data Collection and Structure Determination

The diffraction data of the native and selenomethionine 18-mer crystals were collected on a Rigaku Raxis IV IP detector mounted on a RUH3R rotating anode with multilayer focusing optics for CuKα at 95°K. The data sets were processed and scaled using HKL2000 (Otwinowski and Minor, 1997) (Table S2). The crystals belonged to R3 2 space group and diffracted X-rays up to 3.1 Å. SIR in SOLVE (Terwilliger and Berendzen, 1999) was used to locate three selenium sites. The experimental maps were traced in Coot (Emsley and Cowtan, 2004) and O (Jones et al., 1991) to produce the complete model of the complex. The resulting model was refined using CNS (Brunger et al., 1998) interspersed with manual building.

High-resolution data sets for the 14-mer, 18-mer, and 20-mer crystals were collected at ID-22 and BM-22 beamlines at Advanced Photon Source on a Mar225 or Mar300 CCD detector at 100°K (Table 1).

The data sets were processed and scaled using HKL2000. The structures were solved by molecular replacement and refined using CNS (Table 1).

The nucleic acid conformation was analyzed using programs CURVES (Lavery and Sklenar, 1988) and 3DNA (Lu and Olson, 2003). Structure analyses including superpositions were done in O or MolMol (http://hugin.ethz.ch/wuthrich/software/molmol/). These programs were also used to build a theoretical model of HIV RT, and its energy minimization was performed in CNS (see the Supplemental Data). Surface potentials were calculated with GRASP (Nicholls et al., 1991). Figures were prepared using PyMOL (http://www.pymol.org).

Binding Assays

EMSA and sedimentation equilibrium experiments are described in detail in the Supplemental Data.

RNase H Cleavage Assays

The activity of native and mutant proteins was assayed using a 5′-^{32}P-labeled 12-mer RNA/DNA (see Table S1 for sequences) or poly(rA)/poly(dT) uniformly labeled with α^{32}P-ATP in 50 mM Tris-HCl (pH 7.9), 50 mM NaCl, 5 mM $MgCl_2$ (or 10 mM $MnCl_2$), 1 mM DTT, 20 μg/ml BSA, and 4% glycerol. Aliquots of reaction mixtures were resolved on a 12% TBE polyacrylamide gel and visualized by autoradiography.

Supplemental Data

Supplemental Data include supplemental text, seven figures, three tables, and Supplemental References and can be found with this article online at http://www.molecule.org/cgi/content/full/28/2/264/DC1/.

ACKNOWLEDGMENTS

We thank Dr. R. Craigie for critical reading of the manuscript and L. Eiben for excellent technical assistance. We acknowledge the assistance of the staff of SERCAT beamline at Advanced Photon Source. This research was supported by the Intramural Research Program of the National Institutes of Health, the National Institute of Diabetes and Digestive and Kidney Diseases, the National Institute of Child Health and Human Development, and the Intramural AIDS Targeted Antiviral Program.

Received: May 22, 2007
Revised: July 16, 2007
Accepted: August 13, 2007
Published: October 25, 2007

REFERENCES

Ben-Artzi, H., Zeelon, E., Le-Grice, S.F., Gorecki, M., and Panet, A. (1992). Characterization of the double stranded RNA dependent RNase activity associated with recombinant reverse transcriptases. Nucleic Acids Res. *20*, 5115–5118.

Blain, S.W., and Goff, S.P. (1993). Nuclease activities of Moloney murine leukemia virus reverse transcriptase. Mutants with altered substrate specificities. J. Biol. Chem. *268*, 23585–23592.

Broccoli, S., Rallu, F., Sanscartier, P., Cerritelli, S.M., Crouch, R.J., and Drolet, M. (2004). Effects of RNA polymerase modifications on transcription-induced negative supercoiling and associated R-loop formation. Mol. Microbiol. *52*, 1769–1779.

Brunger, A.T., Adams, P.D., Clore, G.M., DeLano, W.L., Gros, P., Grosse-Kunstleve, R.W., Jiang, J.S., Kuszewski, J., Nilges, M., Pannu, N.S., et al. (1998). Crystallography and NMR system: a new software suite for macromolecular structure determination. Acta Crystallogr. D Biol. Crystallogr. *54*, 905–921.

Cerritelli, S.M., and Crouch, R.J. (1995). The non-RNase H domain of Saccharomyces cerevisiae RNase H1 binds double-stranded RNA: magnesium modulates the switch between double-stranded RNA binding and RNase H activity. RNA *1*, 246–259.

Cerritelli, S.M., and Crouch, R.J. (1998). Cloning, expression, and mapping of ribonucleases H of human and mouse related to bacterial RNase HI. Genomics *53*, 300–307.

Cerritelli, S.M., Frolova, E.G., Feng, C., Grinberg, A., Love, P.E., and Crouch, R.J. (2003). Failure to produce mitochondrial DNA results in embryonic lethality in Rnaseh1 null mice. Mol. Cell *11*, 807–815.

Das, D., and Georgiadis, M.M. (2004). The crystal structure of the monomeric reverse transcriptase from Moloney murine leukemia virus. Structure *12*, 819–829.

DeStefano, J.J., Buiser, R.G., Mallaber, L.M., Myers, T.W., Bambara, R.A., and Fay, P.J. (1991). Polymerization and RNase H activities of the reverse transcriptases from avian myeloblastosis, human immunodeficiency, and Moloney murine leukemia viruses are functionally uncoupled. J. Biol. Chem. *266*, 7423–7431.

Emsley, P., and Cowtan, K. (2004). Coot: model-building tools for molecular graphics. Acta Crystallogr. D Biol. Crystallogr. *60*, 2126–2132.

Furfine, E.S., and Reardon, J.E. (1991). Reverse transcriptase.RNase H from the human immunodeficiency virus. Relationship of the DNA polymerase and RNA hydrolysis activities. J. Biol. Chem. *266*, 406–412.

Gaidamakov, S.A., Gorshkova, I.I., Schuck, P., Steinbach, P.J., Yamada, H., Crouch, R.J., and Cerritelli, S.M. (2005). Eukaryotic RNases H1 act processively by interactions through the duplex RNA-binding domain. Nucleic Acids Res. *33*, 2166–2175.

Gao, H.Q., Boyer, P.L., Arnold, E., and Hughes, S.H. (1998). Effects of mutations in the polymerase domain on the polymerase, RNase H and strand transfer activities of human immunodeficiency virus type 1 reverse transcriptase. J. Mol. Biol. *277*, 559–572.

Gopalakrishnan, V., Peliska, J.A., and Benkovic, S.J. (1992). Human immunodeficiency virus type 1 reverse transcriptase: spatial and temporal relationship between the polymerase and RNase H activities. Proc. Natl. Acad. Sci. USA *89*, 10763–10767.

Haruki, M., Noguchi, E., Kanaya, S., and Crouch, R.J. (1997). Kinetic and stoichiometric analysis for the binding of Escherichia coli ribonuclease HI to RNA-DNA hybrids using surface plasmon resonance. J. Biol. Chem. *272*, 22015–22022.

Hostomsky, Z., Hostomska, Z., Hudson, G.O., Moomaw, E.W., and Nodes, B.R. (1991). Reconstitution in vitro of RNase H activity by using purified N-terminal and C-terminal domains of human immunodeficiency virus type 1 reverse transcriptase. Proc. Natl. Acad. Sci. USA *88*, 1148–1152.

Huang, H., Chopra, R., Verdine, G.L., and Harrison, S.C. (1998). Structure of a covalently trapped catalytic complex of HIV-1 reverse transcriptase: implications for drug resistance. Science *282*, 1669–1675.

Hughes, S.H., Arnold, E., and Hostomsky, Z. (1998). RNase H of retroviral reverse transcriptases. In Ribonucleases H, R.J. Crouch and J.J. Toulme, eds. (Paris: INSERM), pp. 195–224.

Jones, T.A., Zou, J.Y., Cowan, S.W., and Kjeldgaard, M. (1991). Improved methods for building protein models in electron density maps and the location of errors in these models. Acta Crystallogr. A *47*, 110–119.

Katayanagi, K., Miyagawa, M., Matsushima, M., Ishikawa, M., Kanaya, S., Ikehara, M., Matsuzaki, T., and Morikawa, K. (1990). Three-dimensional structure of ribonuclease H from E. coli. Nature *347*, 306–309.

Katayanagi, K., Okumura, M., and Morikawa, K. (1993). Crystal structure of Escherichia coli RNase HI in complex with Mg2+ at 2.8 Å resolution: proof for a single Mg(2+)-binding site. Proteins *17*, 337–346.

Kati, W.M., Johnson, K.A., Jerva, L.F., and Anderson, K.S. (1992). Mechanism and fidelity of HIV reverse transcriptase. J. Biol. Chem. *267*, 25988–25997.

Keck, J.L., and Marqusee, S. (1996). The putative substrate recognition loop of Escherichia coli ribonuclease H is not essential for activity. J. Biol. Chem. *271*, 19883–19887.

Klumpp, K., and Mirzadegan, T. (2006). Recent progress in the design of small molecule inhibitors of HIV RNase H. Curr. Pharm. Des. *12*, 1909–1922.

Kogoma, T., and Foster, P.L. (1998). Physiological functions of *E. coli* RNase HI. In Ribonucleases H, R.J. Crouch and J.J. Toulme, eds. (Paris: INSERM), pp. 39–66.

Kohlstaedt, L.A., Wang, J., Friedman, J.M., Rice, P.A., and Steitz, T.A. (1992). Crystal structure at 3.5 Å resolution of HIV-1 reverse transcriptase complexed with an inhibitor. Science *256*, 1783–1790.

Kopka, M.L., Lavelle, L., Han, G.W., Ng, H.L., and Dickerson, R.E. (2003). An unusual sugar conformation in the structure of an RNA/DNA decamer of the polypurine tract may affect recognition by RNase H. J. Mol. Biol. *334*, 653–665.

Lavery, R., and Sklenar, H. (1988). The definition of generalized helicoidal parameters and of axis curvature for irregular nucleic acids. J. Biomol. Struct. Dyn. *6*, 63–91.

Lim, D., Gregorio, G.G., Bingman, C., Martinez-Hackert, E., Hendrickson, W.A., and Goff, S.P. (2006). Crystal structure of the moloney murine leukemia virus RNase H domain. J. Virol. *80*, 8379–8389.

Lima, W.F., and Crooke, S.T. (1997). Binding affinity and specificity of Escherichia coli RNase H1: impact on the kinetics of catalysis of antisense oligonucleotide-RNA hybrids. Biochemistry *36*, 390–398.

Lima, W.F., Nichols, J.G., Wu, H., Prakash, T.P., Migawa, M.T., Wyrzykiewicz, T.K., Bhat, B., and Crooke, S.T. (2004). Structural requirements at the catalytic site of the heteroduplex substrate for human RNase H1 catalysis. J. Biol. Chem. *279*, 36317–36326.

Lu, X.J., and Olson, W.K. (2003). 3DNA: a software package for the analysis, rebuilding and visualization of three-dimensional nucleic acid structures. Nucleic Acids Res. *31*, 5108–5121.

Nicholls, A., Sharp, K.A., and Honig, B. (1991). Protein folding and association: insights from the interfacial and thermodynamic properties of hydrocarbons. Proteins *11*, 281–296.

Nowotny, M., and Yang, W. (2006). Stepwise analyses of metal ions in RNase H catalysis from substrate destabilization to product release. EMBO J. *25*, 1924–1933.

Nowotny, M., Gaidamakov, S.A., Crouch, R.J., and Yang, W. (2005). Crystal structures of RNase H bound to an RNA/DNA hybrid: substrate specificity and metal-dependent catalysis. Cell *121*, 1005–1016.

Oda, Y., Yoshida, M., and Kanaya, S. (1993). Role of histidine 124 in the catalytic function of ribonuclease HI from Escherichia coli. J. Biol. Chem. *268*, 88–92.

Otwinowski, Z., and Minor, W. (1997). Processing of X-ray diffraction data collected in oscillation mode. In Methods in Enzymology, C.W. Carter and R.M. Sweet, eds. (New York: Academic Press), pp. 307–326.

Palaniappan, C., Fuentes, G.M., Rodriguez-Rodriguez, L., Fay, P.J., and Bambara, R.A. (1996). Helix structure and ends of RNA/DNA hybrids direct the cleavage specificity of HIV-1 reverse transcriptase RNase H. J. Biol. Chem. *271*, 2063–2070.

Purohit, V., Roques, B.P., Kim, B., and Bambara, R.A. (2007). Mechanisms that prevent template inactivation by HIV-1 reverse transcriptase RNase H cleavages. J. Biol. Chem. *282*, 12598–12609.

Rausch, J.W., Qu, J., Yi-Brunozzi, H.Y., Kool, E.T., and Le Grice, S.F. (2003). Hydrolysis of RNA/DNA hybrids containing nonpolar pyrimidine isosteres defines regions essential for HIV type 1 polypurine tract selection. Proc. Natl. Acad. Sci. USA *100*, 11279–11284.

Repaske, R., Hartley, J.W., Kavlick, M.F., O'Neill, R.R., and Austin, J.B. (1989). Inhibition of RNase H activity and viral replication by single mutations in the 3′ region of Moloney murine leukemia virus reverse transcriptase. J. Virol. *63*, 1460–1464.

Rice, P.A., and Baker, T.A. (2001). Comparative architecture of transposase and integrase complexes. Nat. Struct. Biol. *8*, 302–307.

Sarafianos, S.G., Das, K., Tantillo, C., Clark, A.D., Jr., Ding, J., Whitcomb, J.M., Boyer, P.L., Hughes, S.H., and Arnold, E. (2001). Crystal structure of HIV-1 reverse transcriptase in complex with a polypurine tract RNA:DNA. EMBO J. *20*, 1449–1461.

Schultz, S.J., Zhang, M., and Champoux, J.J. (2004). Recognition of internal cleavage sites by retroviral RNases H. J. Mol. Biol. *344*, 635–652.

Shaw-Reid, C.A., Feuston, B., Munshi, V., Getty, K., Krueger, J., Hazuda, D.J., Parniak, M.A., Miller, M.D., and Lewis, D. (2005). Dissecting the effects of DNA polymerase and ribonuclease H inhibitor combinations on HIV-1 reverse-transcriptase activities. Biochemistry *44*, 1595–1606.

Steitz, T.A., and Steitz, J.A. (1993). A general two-metal-ion mechanism for catalytic RNA. Proc. Natl. Acad. Sci. USA *90*, 6498–6502.

Terwilliger, T.C., and Berendzen, J. (1999). Automated MAD and MIR structure solution. Acta Crystallogr. D Biol. Crystallogr. *55*, 849–861.

Tisdale, M., Schulze, T., Larder, B.A., and Moelling, K. (1991). Mutations within the RNase H domain of human immunodeficiency virus type 1 reverse transcriptase abolish virus infectivity. J. Gen. Virol. *72*, 59–66.

Tolia, N.H., and Joshua-Tor, L. (2007). Slicer and the argonautes. Nat. Chem. Biol. *3*, 36–43.

Wu, H., Lima, W.F., and Crooke, S.T. (1999). Properties of cloned and expressed human RNase H1. J. Biol. Chem. *274*, 28270–28278.

Wu, H., Lima, W.F., and Crooke, S.T. (2001). Investigating the structure of human RNase H1 by site-directed mutagenesis. J. Biol. Chem. *276*, 23547–23553.

Yang, W., and Steitz, T.A. (1995). Recombining the structures of HIV integrase, RuvC and RNase H. Structure *3*, 131–134.

Yang, W., Hendrickson, W.A., Crouch, R.J., and Satow, Y. (1990). Structure of ribonuclease H phased at 2 Å resolution by MAD analysis of the selenomethionyl protein. Science *249*, 1398–1405.

Yang, W., Lee, J.Y., and Nowotny, M. (2006). Making and breaking nucleic acids: two-Mg2+-ion catalysis and substrate specificity. Mol. Cell *22*, 5–13.

Accession Numbers

The Protein Data Bank accession codes for the atomic coordinates and structure factors are 2QKK, 2KQ9, and 2QKB for 14-mer RNA/DNA complex, 18-mer complex, and 20-mer complex, respectively.

Molecular Cell
Errata

Structure of Human RNase H1 Complexed with an RNA/DNA Hybrid: Insight into HIV Reverse Transcription

Marcin Nowotny, Sergei A. Gaidamakov, Rodolfo Ghirlando, Susana M. Cerritelli, Robert J. Crouch, and Wei Yang*
*Correspondence: wei.yang@nih.gov
DOI 10.1016/j.molcel.2007.10.021

(Molecular Cell *28*, 264–276; October 26, 2007)
On page 267, the following sentence is incorrect: "Interestingly, the DNA strand is mainly B-like (between C2′-endo and O4′-endo) except for the deoxynucleotide in the DNA-binding channel, which is between A and B form (C4′-exo)." Instead, the sentence should read "Interestingly, the DNA strand is B-like in the phosphate-binding pocket and A-like in the DNA-binding channel."